ACS APPLIED ELECTRONIC MATERIALS

pubs.acs.org/acsaelm Article

High-Resolution Spatial Mapping of Pressure Distribution by a Flexible and Piezotronics Transistor Array

Li Zhang, Yepei Mo, Wenda Ma, Ru Wang, Yixin Wan, Rongrong Bao,* and Caofeng Pan*

Cite This: https://doi.org/10.1021/acsaelm.3c00683 Read Online

ACCESS | Metrics & More | Article Recommendations | Supporting Information

ABSTRACT: The simulation of human tactile through high-resolution electronics will play an essential role in robotics and human−robot interaction. Piezotronic tactile sensors can achieve a higher resolution of mapping and integration than conventional tactile sensors. Herein, we demonstrate a flexible tactile transistor sensing array based on piezotronic zinc oxide (ZnO) nanowires to modulate the carrier concentration directly. When a compressive strain is applied along the *C*-axis of the ZnO nanowire, positive piezoelectric charges will be induced at the channel to increase the concentration of electron carriers. With an applied pressure of 25 N, the current was increased more than 10 times. Moreover, the large-scale transistor array makes mapping of external forces possible. In this study, a flexible pressure sensor was designed with 181 dots per inch (DPI) pixel density. The pressure from a sapphire mold with a "BI" bump pattern was effectively mapped by the current changes of transistors. This study achieved spatially resolved pressure mapping, which has tremendous potential for applications in electronic skin, biomedicine, human−machine interfaces, and micro-nano sensing.

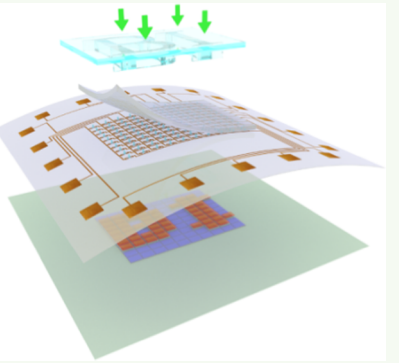

KEYWORDS: *piezotronic effect, zinc oxide, field-effect transistors, piezoelectricity, array*

INTRODUCTION

The ability to perceive external physical information using electronics is a significant challenge in human−computer interaction. Force sensors play an important role in the detection of various physical signals. Currently, there are many different types of force sensors, each with its own limitations.[1−13] Flexibility, spatial resolution, and sensitivity are still limitations in the field of human−computer interaction. There are five types of force sensors based on their operating principles: resistive,[5,14] capacitive, field-effect transistor,[15−17] friction, and piezoelectric.[10,18−20] Sensors based on resistance or capacitance have been developed earlier and are more mature; however, it is more difficult to achieve a high spatial resolution.[21,22] Force sensors based on field-effect transistor structures often require the combination of other pressure-sensitive materials, which makes circuit design difficult and expensive. External force senses based on friction have a slow response time and poor interference immunity. The research group of Professor Zhonglin Wang proposed the basic concepts and principles of piezoelectric electronics and piezoelectric optoelectronics in 2007 and 2010, respectively.[9] Because piezoelectric materials possess the property that when subjected to an external force, the piezoelectric potential can effectively modulate the carrier transport properties at the semiconductor interface.[7,10,18,23−30] As a result, it is possible to achieve a high spatial resolution of external forces by using piezoelectric properties. By modulating the height of the Schottky barrier between zinc oxide and metal by piezoelectric potential, piezoelectric electronics-based pressure sensors achieved 254 dots per inch (DPI) pressure resolution in 2013[28] and increased it to 12,700[31−40] DPI in 2017.[20,38] However, piezoelectric pressure sensors that directly modulate carrier concentration through piezoelectric potential and achieve high resolution and flexibility have been less explored.

Due to the noncentrosymmetric structure of ZnO with a wurtzite structure, a piezoelectric potential is generated at both ends of the *C*-axis when an external force is applied along that axis. As a result of many defects, polycrystalline ZnO films prepared on substrates by magnetron sputtering exhibit N-type semiconductor properties.[38] Magnetron sputtered ZnO is used as a channel material on a flexible positron emission tomography (PET) substrate. By modulation of the concentration of electron carriers at channel locations with the help of the piezoelectric potential generated by hydrothermally grown ZnO nanowires under external stress, high-resolution imaging of forces can be achieved.

In contrast to conventional field-effect transistors, this design regulates the carrier concentration directly at the channel location by using a piezoelectric potential. It is noted that the

Received: May 23, 2023
Accepted: August 13, 2023

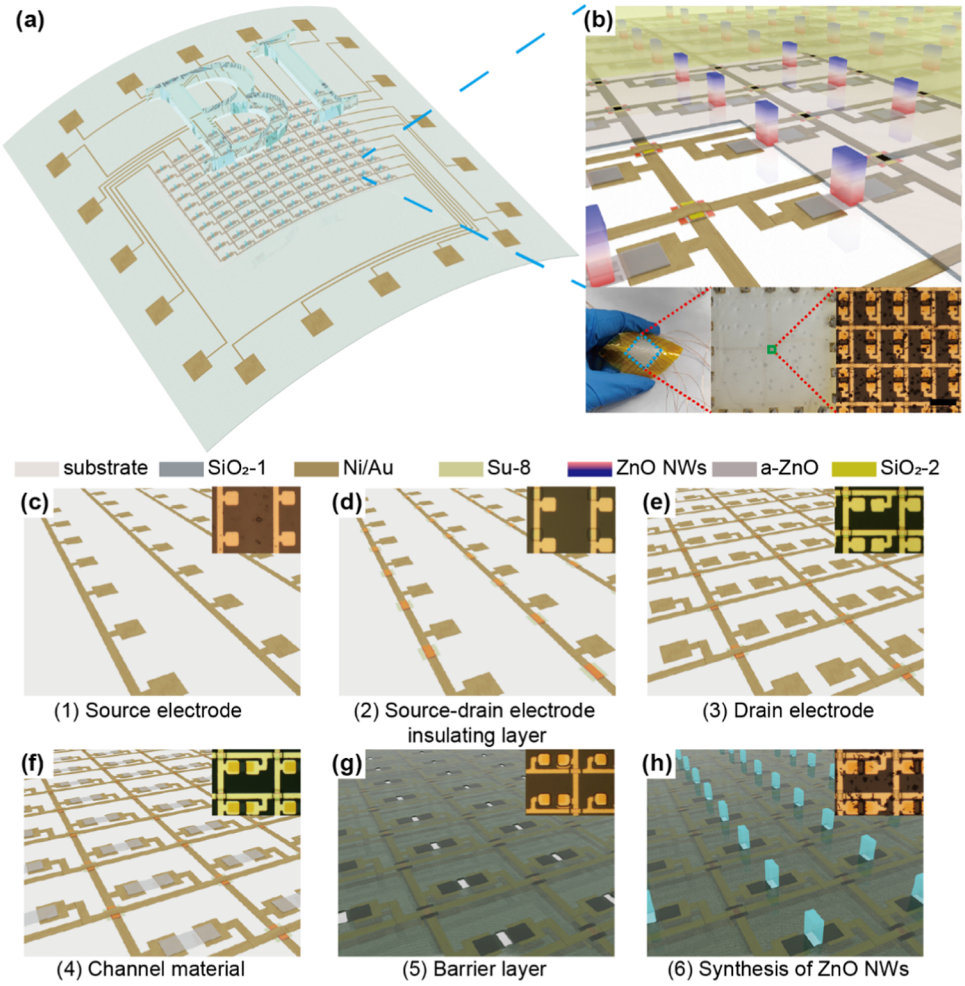

Figure 1. ZnO-PGPT array device structure diagram, optical photos, and fabrication process. (a) Schematic structure of the ZnO-PGPT array device with the functional region of the array device enlarged (b) to show its specific details (inset is a physical picture of the device). Structure and physical optical images (inset) of functional regions taken during array device preparation (c–h). The scale bar is 100 μm.

pressure-gate piezotronic transistors (PGPT) sensor, unlike the previously described technique of modulating the height structure of the Schottky barrier between metal and semiconductor, is easier to integrate with other circuits and can achieve a resolution mapping of the pressure of up to 7143/cm^2 (181 DPI), higher than the resolution of the human fingertip, which is 241/cm^2 (40 DPI).[39] By the use of a flexible PET substrate, the array of pressure sensors can be applied to a broader range of applications. Our research is the first to achieve flexible high-resolution pressure mapping using a variety of piezoelectric transistors with a piezoelectric potential that controls the concentration of electrons in the channel.

RESULTS AND DISCUSSION

The structure of an array of pressure-gate piezoelectric transistors (PGPT) is shown in Figure 1a. The pressure distribution sensing area is composed of a 10 × 10 pixels ZnO-PGPT array prepared on a flexible PET substrate (a schematic diagram of the device is shown in Figure 1b). The test instrument is connected to the functional area through a circuit design. Upon applying external pressure to the ZnO nanowires at the pixel sites in the functional region, a positive piezoelectric potential is generated, which increases the concentration of electron carriers owing to piezoelectric effects. Thus, the ZnO-PGPT array is capable of high-spatial-resolution pressure mapping through current variation at a fixed bias. The insets of Figure 1b are photos and a microscope photo of devices. The device preparation process is shown in Figure 1c–1h. First, source electrodes are prepared on the flexible substrate with a line width of 10 μm, spaced 140 μm apart (Figure 1c). Second, an insulating layer is constructed at the source–drain electrode crossover point to isolate the source–drain electrode (Figure 1d). Third, a drain electrode with a line width of 10 μm arranged 100 μm apart is prepared at the corresponding position (Figure 1e). Fourth, a polycrystalline ZnO material with a channel length and width of 20 × 20 μm^2 is prepared by magnetron sputtering between the source and drain electrodes (Figure 1f). Fifth, silicon oxide was used to cover the polycrystalline ZnO, apart from the 10 × 20 μm^2 area in the center (Figure 1g). Sixth, ZnO nanowires were grown vertically by a peristaltic pump using a hydrothermal method in polycrystalline ZnO regions without areas of silicon oxide (Figure 1h). Finally, the functional region is encapsulated with an SU8 photoresist (Figure 1b, inset). Detailed flow is provided in the Supporting Information.

According to ZnO nanowire piezoelectric potential modulation regions, two types of devices were designed. In device 1, ZnO nanowires are present only at the center of the channel

https://doi.org/10.1021/acsaelm.3c00683
ACS Appl. Electron. Mater. XXXX, XXX, XXX–XXX

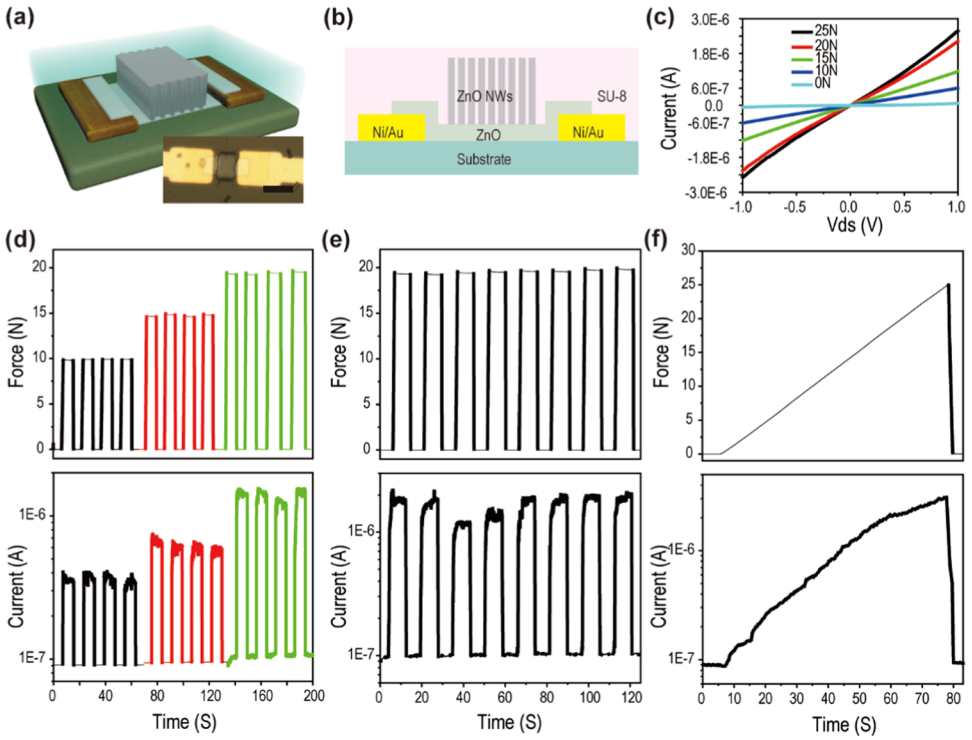

Figure 2. Structure of device 1, optical photos, and pressure regulation tests. (a) Structural and optical photographs of device 1 (inset) and structural demonstration of the device side (b). Source leakage current of the device at constant pressure (c). Response (d) of device 1 when different cyclic forces are applied to the device using a tensioning machine. Electrical characteristics of the sensor when a periodic pressure of 20 N is applied (e). The variation of the source leakage current when a uniformly increasing force is applied (f). Both cyclic pressure and uniformly increasing pressure are applied to the device with 1 V bias. The scale bar is 20 μm.

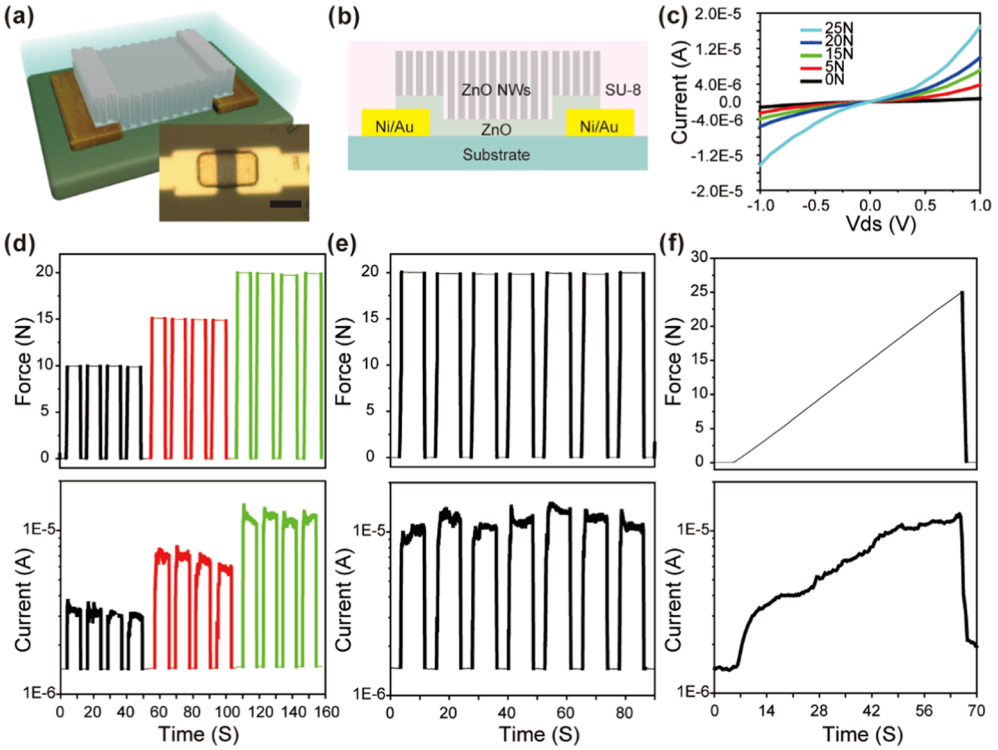

Figure 3. Structure of device 2, optical photos, and pressure regulation tests. (a) Structural and optical photographs of device 1 (inset) and (b) structural demonstration of the device side. Source leakage current of the device at constant pressure (c). It shows the response (d) of device 2 when different cyclic forces are applied to the device using a tensioning machine. Electrical characteristics of the sensor when a periodic pressure of 20 N is applied (e). The variation of the source leakage current when a uniformly increasing force is applied (f). Both cyclic pressure and uniformly increasing pressure are applied to the device with 1 V bias. The scale bar is 20 μm.

https://doi.org/10.1021/acsaelm.3c00683
ACS Appl. Electron. Mater. XXXX, XXX, XXX−XXX

material. In device 2, ZnO nanowires cover all polycrystalline ZnO films.

ELECTRICAL PROPERTIES OF DEVICE 1

The first type of ZnO-PGPT device was designed by us. First, the Ni/Au metal is used as the source−drain electrode, and polycrystalline ZnO is used as the channel material. Hydrothermal method is used to grow ZnO nanowires in the center of the channel. Finally, the device part is encapsulated using an SU8 photoresist (the physical picture is shown in the inset of Figure 2a). Unlike the field regulation characteristics of conventional field-effect transistors, the PGPT produces negative and positive piezoelectric potentials, respectively, at the top and bottom of the ZnO nanowires when the Structure 1 device is compressed. Due to the piezoelectric potential generated by the ZnO nanowires, the carriers (electron) move in the direction of the positive potential (bottom), so the current increases with increasing pressure when Structure 1 is loaded with a fixed bias. To examine the piezoelectric regulation of Structure 1 devices, we applied constant pressure to the device with a three-dimensional (3D) displacement stage while testing their electrical characteristics with a Keysight 1500 semiconductor analyzer. The electrical features of device 1 under continual stress are shown in Figure 2c. With a bias voltage of 1 V, the source leakage current increases with increasing pressure. The tensile testing machine YL-S71 produced by Guangdong Yue Lian Instrument Co., Ltd. was used to apply periodic pressure to the device, while the current of the device was measured in real time using a semiconductor analyzer 4200. By applying 10, 15, and 20 N pressure to the device (Figure 2d), different strains can be distinguished by measuring the current at the 1 V bias. When an external bias voltage of 1 V is applied to the device (Figure 2e), the source leakage current increases by more than 10 times with excellent repeatability if a periodic pressure of 20 N is applied. This is similar to the transfer curves for field-effect transistors. A stretching machine was used to apply linearly increasing pressure from 0 to 25 N to device 1, while a Keithley 4200 was used to test the electrical characteristics of the device. Increasing the pressure on device 1 causes the current to gradually increase, and at 25 N, the current increases 18 times in comparison to not having any pressure applied (Figure 2f).

ELECTRICAL PROPERTIES OF DEVICE 2

The PGPT device 2 that we have designed differs from device 1 shown in Figure 3a,b. First, magnetron sputtered Ni/Au was used as the source−drain metal electrode. Second, a polycrystalline ZnO film was fabricated using magnetron sputtering as the channel material. Third, ZnO nanowires were grown vertically on the polycrystalline ZnO films using the hydrothermal method. Finally, the devices are encapsulated using an Su8 photoresist. The physical image of device 2 is shown in the inset of Figure 3a (the detailed flow is shown in Figure S2). The piezoelectric potential generated by device 2 ZnO nanowires when subjected to pressure can modulate more structures than device 1. Further discussion of the change in conductivity of device 2 after being subjected to pressure is provided in the next section. The electrical properties of device 2 when subjected to a fixed stress are shown in Figure 3c, which is similar to the output curve of a conventional field-effect transistor. In order to apply constant stresses on device 2, a 3D displacement table was used. At the same time, 1500 lx was used to test the device source leakage current. When subjected to pressure, the current of device 2 can increase from 6.85×10^{-7}Å (0 N) to 1.7×10^{-5}Å (25 N). Considering that the pressure sensor can respond to external forces, we tested its repeatability under periodic external forces (as shown in Figure 3d,e) and found that the device demonstrated good repeatability as well as good discrimination between different sources of force. Finally, similar to the field-effect transistor transfer curve, we applied linearly increasing pressure on the device two at 1 V bias with the same measured current that can be grown between 1.41×10^{-6} Å (0 N) and 1.27×10^{-5} Å (25 N) (Figure 3f). After releasing the external force, the device is able to restore the current to its initial state.

PIEZOELECTRIC POTENTIAL MODULATION

According to the piezoelectric theory and using energy band diagrams, we can explain the reason for the current variation with external stress for both devices 1 and 2, as shown in Figure 4. Device 1 has a structure as shown in Figure 4a, where a polycrystalline ZnO film is used as the channel material, and ZnO nanowires are grown perpendicularly in the middle of the channel by controlling the growth area. By analyzing this structure, it can be seen that if a fixed bias voltage is applied to device 1, electrons form a circuit through the source electrode, ZnO film, ZnO nanowire mixed material, and drain electrode. Neglecting the difference in the Fermi level between the ZnO film and the ZnO nanowire caused by factors such as specific

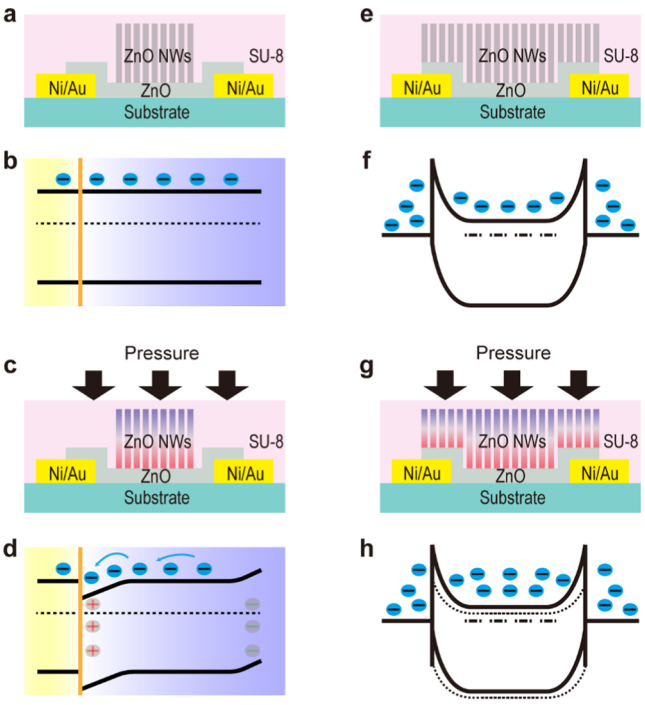

Figure 4. Illustration of the mechanism by which the current increases with increasing pressure when two devices are subjected to pressure. Structure (a) and energy band diagram (b) of device 1 without pressure. ZnO nanowires generate a negative and positive piezoelectric potential due to pressure at the top and bottom, respectively (c), accompanied by a change in the energy band (d). Structure (e) and energy band diagram (f) of device 2 without pressure. ZnO nanowires generate a negative and positive piezoelectric potential due to pressure at the top and bottom, respectively (g), accompanied by a change in energy band (h).

https://doi.org/10.1021/acsaelm.3c00683
ACS Appl. Electron. Mater. XXXX, XXX, XXX−XXX

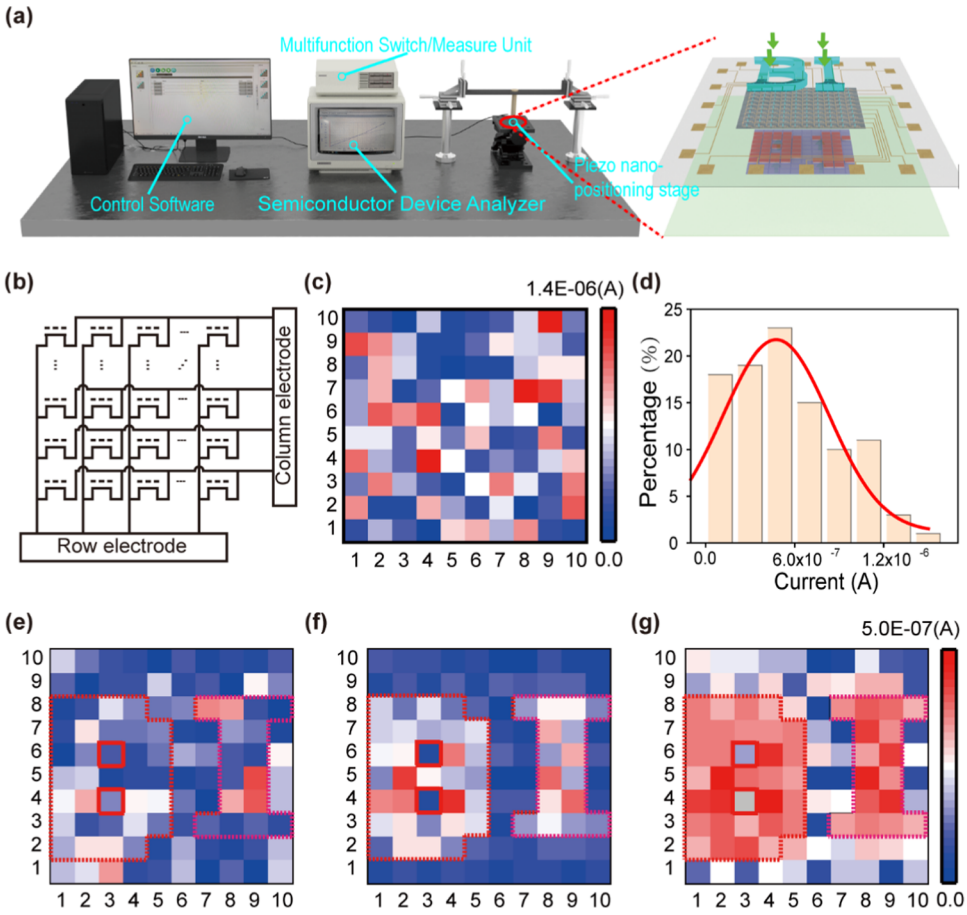

Figure 5. Test bench and ZnO-PGPT array sensor prepared using device 1 structure are used for high-resolution pressure testing. (a) Test bench for array devices. Moving up the displacement stage applies pressure to the device, and the electrical test system measures the current at each pixel. In order to simulate a pressure distribution in a tiny area, sapphire is used with a "BI" bump to apply pressure to the array device. Circuit diagram of the sensor (b). Multichannel system used to test the initial current of the pressure sensor (c). Initial current statistics for array devices (d). (e–g) Increase in current after applying 10, 30, and 50 N to the device, respectively.

surface area, the band structure of the contact position between the ZnO film and the ZnO nanowire is shown in Figure 4b, and the electrons in the ZnO nanowire are uniformly distributed. Due to the piezoelectric potential generated in the ZnO nanowire after it is subjected to pressure, the electron carrier distribution inside the nanowire will be redistributed[40] (electrons will aggregate toward the positive piezoelectric potential end and move away from the negative piezoelectric potential end). Simulations using COMSOL on a bundle of ZnO nanowires aligned along the *C*-axis reveal that a negative piezoelectric potential will be generated at the top and a positive piezoelectric potential at the bottom of the nanowire under pressure (see Figure S9). Therefore, when device 1 is subjected to stress (Figure 4c), the electron carrier concentration at the position toward the ZnO film increases, as electrons in the ZnO nanowires migrate toward the ZnO film, resulting in an increase in the electron concentration at that location (Figure 4d). Thus, applying external pressure to device 1 under a fixed bias voltage will increase the current flowing between the source and drain electrodes.

Device 2 is distinct from device 1 in that the ZnO nanowires in device 2 cover the entire polycrystalline ZnO film (as shown in Figure 4e). Under no pressure, the band structure of device 2 is illustrated in Figure 4f, where Schottky contacts form between the source–drain metal electrodes and the ZnO film. Meanwhile, the electrons in the ZnO film and the ZnO nanowire mixed layer between the source and drain electrodes are evenly distributed. Due to the piezoelectric effect, which can regulate the Schottky barrier between the piezoelectric semiconductor and metal,[41] when device 2 is subjected to pressure, a positive piezoelectric potential is generated at the bottom of the ZnO nanowire (Figure 4g). This effect not only causes the ZnO film and ZnO nanowire mixed layer between the source and drain electrodes to have the same effect as device 1 but also lowers the Schottky barrier between the source–drain electrodes and ZnO (as indicated by the dashed line in Figure 4h). Consequently, under a fixed bias, applying pressure to device 2 leads to an increase in the current between the source and drain electrodes.

PRESSURE MAPPING

Based on the structure of device 1, we created a 10 × 10 PGPT array pressure sensor with 181 DPI (7143/cm2) pixel density. A detailed description of the preparation process for the sensor array can be found in Figure S3. For the purpose of testing the mapping of PGPT to pressure, a sapphire with a "BI" bump is placed on the device surface and pressure is applied to simulate tiny area pressure distributions. The testbed is shown in Figure 5a. A cantilever fixed to a three-dimensional displacement table is used to apply pressure to the PGPT array devices. A PC

https://doi.org/10.1021/acsaelm.3c00683
ACS Appl. Electron. Mater. XXXX, XXX, XXX–XXX

connected to an eyesight 1500 semiconductor device analyzer controls the multifunction switch unit in order to collect current data at the relevant positions of the array devices. Drawings accompanying Figure 5a illustrate the PGPT array device test schematic. Under an optical microscope, sapphire with a "BI" bump pattern is aligned with the PGPT array device. In order to record the pressure applied, the PGPT array device is placed on an electronic scale. One-dimensional displacement tables are moved up and down to obtain different pressures. In the array device, the current of pixels covered by sapphire bumps increases due to the piezoelectric effect and is different from the current of pixels uncovered. The equivalent circuit diagram for the PGPT array device is shown in Figure 5b. Figure 5c shows the initial currents of the array devices measured by using the test bench. For the array devices, the majority of the initial currents were distributed at $5 \times 10 \times 10^{-7}$Å as shown in Figure 5d. As shown in Figure 5e,f, the current increases after applying 10, 30, and 50 N pressure to the device. With increasing pressure, the current change of the pixel at the "BI" position gradually increases, allowing it to be distinguished from the other pixels. Through the variation of the current, a high spatial resolution of pressure can be obtained.

CONCLUSIONS

In summary, the PGPT device measures pressure by changing the piezoelectric potential when pressure is applied. According to the piezoelectric potential regulation range, PGPT can be classified into two types: a type of device in which the piezoelectric potential only impacts carrier concentration at a channel location and a type of device in which the piezoelectric potential influences both carrier concentration (device 1) and the Schottky barrier height between the channel material and the source−drain electrode (device 2). For both types of devices, the current increased more than 10 times when subjected to 24 N pressure compared to no pressure. When both types of devices are subject to periodic pressure, the difference in the current can be used in order to distinguish the pressures when a fixed amount of voltage is applied, and the current can return to the original level after the pressure has been released. A key characteristic of device 1 is the small initial current, which leads to reduced energy consumption, and the piezoelectric potential, which affects only the carrier concentration at the channel position. A 10 × 10 PGPT array device prepared and designed based on the device 1 structure has spatial resolutions of 140 μm in the X-axis direction and 100 μm in the Y-axis direction. Finally, the "BI" bumps on the surface of sapphire are used to apply pressure to the array device and map the pressure by reading the change in pixel current of the array device. In this work, piezoelectric transistors on a flexible substrate are used to map pressure at a high resolution. It provides new ideas for applications in human−computer interaction, robotics, and other fields where pressure sensing is required.

EXPERIMENTAL SECTION

Fabrication of Devices 1 and 2. The substrates were ultrasonically cleaned with alcohol, acetone, and deionized water. And then the substrates were dried in an oven at 70 °C after removing most of the attached water with compressed air (structure diagram Figure S1a). Second, the prepared substrate was photolithographed to obtain the desired source−drain pattern of the photoresist. The source−drain Ni/Au electrodes were then fabricated by magnetron sputtering (70 W, 3 min). After cleaning the photoresist with acetone, the source−drain electrode pattern of device 1 was obtained, as shown in Figure S1b (structure diagram) and Figure S1g (optical photograph). Through the second photolithography combined with magnetron sputtering (70 W, 30 min), a polycrystalline ZnO film was obtained between the source and drain electrodes in Figure S1c (structure diagram) and Figure S1h (optical photograph). Similar to the previous step, third lithography and magnetron sputtering were applied (300 W, 10 min) to cover all polycrystalline ZnO films except the central 10 × 20 μm^2 region (shown in Figures S1d,i). Additionally, ZnO nanowire bundles were grown by hydrothermal methods (see the Growth of ZnO Nanowires by Hydrothermal Methods Section for details) on the central 10 × 20 μm^2 region of exposed polycrystalline ZnO films (shown in Figure S1e,j,k (projected light photo)). Finally, device 1 was encapsulated using an SU8 photoresist (Figure S1f). Noteworthy, device 2 was fabricated similarly to device 1, except that it was not covered with silica, so ZnO nanowires were grown in all areas of the polycrystalline ZnO film (shown in Figure S2).

Fabrication of the PGPT Array Devices. The PGPT array devices are fabricated on a PET substrate. Through photolithography combined with magnetron sputtering, a source electrode pattern can be obtained (Figure S3b). Through second lithography, magnetron sputtering of SiO_2 (300 W, 2 h) provides an insulating layer at the intersection of the source and drain (Figure S3c). And the drain electrode was made by magnetron sputtering of Ni/Au (Figure S3d) by the third lithography process. And then, the preparation of polycrystalline ZnO film and hydrothermal growth of ZnO nanowires are similar to that of device 1 (Figure S3f−h). The array of devices is depicted in Figure S3i.

Growth of ZnO Nanowires by Hydrothermal Methods. For the growth of ZnO nanowires, the substrate was placed into solution (800 mL) of zinc nitrate hexahydrate (40 mM) and hexamethylenetetramine (40 mM) for 1 h (Figure S6b). An additional 2 L of zinc nitrate hexahydrate and hexamethylenetetramine solution was pumped into the reaction vessel by the peristaltic pump (Figure S6a). In order to maintain a stable volume of solution in the reaction vessel, the solution was pumped in the reaction vessel, while the solution was pumped out by the other peristaltic pump. The reaction vessel was maintained at a constant temperature of 85 °C throughout the whole growth process, which lasted about 24 h.

ASSOCIATED CONTENT

Supporting Information

The Supporting Information is available free of charge at https://pubs.acs.org/doi/10.1021/acsaelm.3c00683.

Schematic diagrams of the fabrication steps for devices 1 and 2 and the corresponding optical photographs for each step; schematic diagrams of the fabrication steps for PGPT array devices; an SU8 photoresist was used to replace the ZnO nanowire growth area in the device 1 structure and the electrical properties of the device were tested after it had been stressed; electrical properties of polycrystalline ZnO thin-film field-effect transistors; growth of ZnO nanowires by hydrothermal methods; SEM image of PGPT array device after growth of ZnO nanowires; photoluminescence spectra of ZnO nanowires; simulation of the distribution of piezoelectric potential in a bundle of zinc oxide nanowires under pressure using COMSOL; XRD spectrum of ZnO nanowires; single device with the structures of devices 1 and 2 underwent 50 cycles of repeatability testing; and comparison between our PGPT-based pressure sensor array and reported studies on pressure detection using piezoelectric potential (PDF)

https://doi.org/10.1021/acsaelm.3c00683
ACS Appl. Electron. Mater. XXXX, XXX, XXX−XXX

AUTHOR INFORMATION

Corresponding Authors

Rongrong Bao − *School of Chemistry and Chemical Engineering, Guangxi University, Nanning, Guangxi 530004, P. R. China; CAS Center for Excellence in Nanoscience, Beijing Key Laboratory of Micro-nano Energy and Sensor, Beijing Institute of Nanoenergy and Nanosystems, Chinese Academy of Sciences, Beijing 101400, P. R. China; School of Nanoscience and Engineering, University of Chinese Academy of Sciences, Beijing 100049, P. R. China*; Email: baorongrong@binn.cas.cn

Caofeng Pan − *School of Chemistry and Chemical Engineering, Guangxi University, Nanning, Guangxi 530004, P. R. China; CAS Center for Excellence in Nanoscience, Beijing Key Laboratory of Micro-nano Energy and Sensor, Beijing Institute of Nanoenergy and Nanosystems, Chinese Academy of Sciences, Beijing 101400, P. R. China; School of Nanoscience and Engineering, University of Chinese Academy of Sciences, Beijing 100049, P. R. China*; orcid.org/0000-0001-6327-9692; Email: cfpan@binn.cas.cn

Authors

Li Zhang − *School of Chemistry and Chemical Engineering, Guangxi University, Nanning, Guangxi 530004, P. R. China; CAS Center for Excellence in Nanoscience, Beijing Key Laboratory of Micro-nano Energy and Sensor, Beijing Institute of Nanoenergy and Nanosystems, Chinese Academy of Sciences, Beijing 101400, P. R. China*

Yepei Mo − *CAS Center for Excellence in Nanoscience, Beijing Key Laboratory of Micro-nano Energy and Sensor, Beijing Institute of Nanoenergy and Nanosystems, Chinese Academy of Sciences, Beijing 101400, P. R. China; School of Nanoscience and Engineering, University of Chinese Academy of Sciences, Beijing 100049, P. R. China*

Wenda Ma − *CAS Center for Excellence in Nanoscience, Beijing Key Laboratory of Micro-nano Energy and Sensor, Beijing Institute of Nanoenergy and Nanosystems, Chinese Academy of Sciences, Beijing 101400, P. R. China*

Ru Wang − *CAS Center for Excellence in Nanoscience, Beijing Key Laboratory of Micro-nano Energy and Sensor, Beijing Institute of Nanoenergy and Nanosystems, Chinese Academy of Sciences, Beijing 101400, P. R. China*

Yixin Wan − *CAS Center for Excellence in Nanoscience, Beijing Key Laboratory of Micro-nano Energy and Sensor, Beijing Institute of Nanoenergy and Nanosystems, Chinese Academy of Sciences, Beijing 101400, P. R. China; School of Nanoscience and Engineering, University of Chinese Academy of Sciences, Beijing 100049, P. R. China*

Complete contact information is available at: https://pubs.acs.org/10.1021/acsaelm.3c00683

Notes

The authors declare no competing financial interest.

ACKNOWLEDGMENTS

The authors thank the support of Natural Science Foundation of Beijing Municipality (L223006, 2222088, Z180011), National Key R&D Project from the Minister of Science and Technology, China (2021YFB3200302 and 2021YFB3200304), National Natural Science Foundation of China (U20A20166, 52192610, 61805015, 52125205, and 61804011), Shenzhen Science and Technology Program (grant no. KQTD20170810105439418), and the Fundamental Research Funds for the Central Universities.

ABBREVIATIONS

ZnO, zinc oxide; DPI, dots per inch; PGPT, pressure-gate piezotronic transistors

REFERENCES

(1) Bauer, S.; Bauer-Gogonea, S.; Graz, I.; Kaltenbrunner, M.; Keplinger, C.; Schwodiauer, R. 25th anniversary article: A soft future: from robots and sensor skin to energy harvesters. *Adv. Mater.* **2014**, *26* (1), 149−161.

(2) Dahiya, R. S.; Metta, G.; Valle, M.; Sandini, G. Tactile Sensing-From Humans to Humanoids. *IEEE Trans. Rob.* **2010**, *26* (1), 1−20.

(3) Hammock, M. L.; Chortos, A.; Tee, B. C. K.; Tok, J. B. H.; Bao, Z. 25th Anniversary Article: The Evolution of Electronic Skin (E-Skin): A Brief History, Design Considerations, and Recent Progress. *Adv. Mater.* **2013**, *25* (42), 5997−6037.

(4) Liu, Y.; Bao, R.; Tao, J.; Li, J.; Dong, M.; Pan, C. Recent progress in tactile sensors and their applications in intelligent systems. *Sci. Bull.* **2020**, *65* (1), 70−88.

(5) Wang, C.; Pan, C.; Wang, Z. Electronic Skin for Closed-Loop Systems. *ACS Nano* **2019**, *13* (11), 12287−12293.

(6) Guo, W.; Xu, C.; Zhu, G.; Pan, C.; Lin, C.; Wang, Z. L. Optical-fiber/TiO2-nanowire-arrays hybrid structures with tubular counter-electrode for dye-sensitized solar cell. *Nano Energy* **2012**, *1* (1), 176−182.

(7) Han, X.; Du, W.; Yu, R.; Pan, C.; Wang, Z. L. Piezo-Phototronic Enhanced UV Sensing Based on a Nanowire Photodetector Array. *Adv. Mater.* **2015**, *27* (48), 7963−7969.

(8) Li, F.; Lu, J.; Zhang, Q.; Peng, D.; Yang, Z.; Xu, Q.; Pan, C.; Pan, A.; Li, T.; Wang, R. Controlled fabrication, lasing behavior and excitonic recombination dynamics in single crystal CH(3)NH(3)-PbBr(3) perovskite cuboids. *Sci. Bull.* **2019**, *64* (10), 698−704.

(9) Pan, C.; Zhai, J.; Wang, Z. L. Piezotronics and Piezo-phototronics of Third Generation Semiconductor Nanowires. *Chem. Rev.* **2019**, *119* (15), 9303−9359.

(10) Pan, C.; Dong, L.; Zhu, G.; Niu, S.; Yu, R.; Yang, Q.; Liu, Y.; Wang, Z. L. High-resolution electroluminescent imaging of pressure distribution using a piezoelectric nanowire LED array. *Nat. Photonics* **2013**, *7* (9), 752−758.

(11) Qiao, S.; Liu, J.; Fu, G.; Ren, K.; Li, Z.; Wang, S.; Pan, C. ZnO nanowire based CIGS solar cell and its efficiency enhancement by the piezo-phototronic effect. *Nano Energy* **2018**, *49*, 508−514.

(12) Wan, B.; Guo, S.; Sun, J.; Zhang, Y.; Wang, Y.; Pan, C.; Zhang, J. Investigating the interlayer electron transport and its influence on the whole electric properties of black phosphorus. *Sci. Bull.* **2019**, *64* (4), 254−260.

(13) Yu, R.; Niu, S.; Pan, C.; Wang, Z. L. Piezotronic effect enhanced performance of Schottky-contacted optical, gas, chemical and biological nanosensors. *Nano Energy* **2015**, *14*, 312−339.

(14) Hua, Q.; Sun, J.; Liu, H.; Bao, R.; Yu, R.; Zhai, J.; Pan, C.; Wang, Z. L. Skin-inspired highly stretchable and conformable matrix networks for multifunctional sensing. *Nat. Commun.* **2018**, *9* (1), No. 244.

(15) Oh, J. Y.; Bao, Z. Second Skin Enabled by Advanced Electronics. *Adv. Sci.* **2019**, *6* (11), No. 1900186.

(16) Someya, T.; Kato, Y.; Sekitani, T.; Iba, S.; Noguchi, Y.; Murase, Y.; Kawaguchi, H.; Sakurai, T. Conformable, flexible, large-area networks of pressure and thermal sensors with organic transistor active matrixes. *Proc. Natl. Acad. Sci. U.S.A.* **2005**, *102* (35), 12321−12325.

(17) Someya, T.; Sekitani, T.; Iba, S.; Kato, Y.; Kawaguchi, H.; Sakurai, T. A large-area, flexible pressure sensor matrix with organic field-effect transistors for artificial skin applications. *Proc. Natl. Acad. Sci. U.S.A.* **2004**, *101* (27), 9966−9970.

(18) Chen, L.; Xue, F.; Li, X.; Huang, X.; Wang, L.; Kou, J.; Wang, Z. L. Strain-Gated Field Effect Transistor of a MoS2-ZnO 2D-1D Hybrid Structure. *ACS Nano* **2016**, *10* (1), 1546−1551.
(19) Dagdeviren, C.; Su, Y.; Joe, P.; Yona, R.; Liu, Y.; Kim, Y. S.; Huang, Y.; Damadoran, A. R.; Xia, J.; Martin, L. W.; Huang, Y.; Rogers, J. A. Conformable amplified lead zirconate titanate sensors with enhanced piezoelectric response for cutaneous pressure monitoring. *Nat. Commun.* **2014**, *5*, No. 4496.
(20) Wang, L.; Liu, S.; Feng, X.; Xu, Q.; Bai, S.; Zhu, L.; Chen, L.; Qin, Y.; Wang, Z. L. Ultrasensitive Vertical Piezotronic Transistor Based on ZnO Twin Nanoplatelet. *ACS Nano* **2017**, *11* (5), 4859−4865.
(21) Liu, X.; Zhang, F.; Huang, R.; Pan, C.; Zhu, J. Capping Modes in PVP-Directed Silver Nanocrystal Growth: Multi-Twinned Nanorods versus Single-Crystalline Nano-Hexapods. *Cryst. Growth Des.* **2008**, *8* (6), 1916−1923.
(22) Xia, K.; Wu, W.; Zhu, M.; Shen, X.; Yin, Z.; Wang, H.; Li, S.; Zhang, M.; Wang, H.; Lu, H.; Pan, A.; Pan, C.; Zhang, Y. CVD growth of perovskite/graphene films for high-performance flexible image sensor. *Sci. Bull.* **2020**, *65* (5), 343−349.
(23) Bao, R. R.; Wang, C. F.; Dong, L.; Shen, C. Y.; Zhao, K.; Pan, C. F. CdS nanorods/organic hybrid LED array and the piezo-phototronic effect of the device for pressure mapping. *Nanoscale* **2016**, *8* (15), 8078−8082.
(24) Bao, R.; Wang, C.; Dong, L.; Yu, R.; Zhao, K.; Wang, Z. L.; Pan, C. Flexible and Controllable Piezo-Phototronic Pressure Mapping Sensor Matrix by ZnO NW/p-Polymer LED Array. *Adv. Funct. Mater.* **2015**, *25* (19), 2884−2891.
(25) Bao, R.; Wang, C.; Peng, Z.; Ma, C.; Dong, L.; Pan, C. Light-Emission Enhancement in a Flexible and Size-Controllable ZnO Nanowire/Organic Light-Emitting Diode Array by the Piezotronic Effect. *ACS Photonics* **2017**, *4* (6), 1344−1349.
(26) Han, W. H.; Zhou, Y. S.; Zhang, Y.; Chen, C. Y.; Lin, L.; Wang, X.; Wang, S. H.; Wang, Z. L. Strain-Gated Piezotronic Transistors Based on Vertical Zinc Oxide Nanowires (vol 6, pg 3760, 2012). *ACS Nano* **2012**, *6* (6), 5736.
(27) Peng, Y. Y.; Que, M. L.; Lee, H. E.; Bao, R. R.; Wang, X. D.; Lu, J. F.; Yuan, Z. Q.; Li, X. Y.; Tao, J.; Sun, J. L.; Zhai, J. Y.; Lee, K. J.; Pan, C. F. Achieving high-resolution pressure mapping via flexible GaN/ZnO nanowire LEDs array by piezo-phototronic effect. *Nano Energy* **2019**, *58*, 633−640.
(28) Wu, W.; Wen, X.; Wang, Z. L. Taxel-addressable matrix of vertical-nanowire piezotronic transistors for active and adaptive tactile imaging. *Science* **2013**, *340* (6135), 952−957.
(29) Zhao, Z. F.; Pu, X.; Han, C. B.; Du, C. H.; Li, L. X.; Jiang, C. Y.; Hu, W. G.; Wang, Z. L. Piezotronic Effect in Polarity-Controlled GaN Nanowires. *ACS Nano* **2015**, *9* (8), 8578−8583.
(30) Zhou, Y. S.; Wang, K.; Han, W. H.; Rai, S. C.; Zhang, Y.; Ding, Y.; Pan, C. F.; Zhang, F.; Zhou, W. L.; Wang, Z. L. Vertically Aligned CdSe Nanowire Arrays for Energy Harvesting and Piezotronic Devices. *ACS Nano* **2012**, *6* (7), 6478−6482.
(31) Hu, G.; Zhou, R.; Yu, R.; Dong, L.; Pan, C.; Wang, Z. L. Piezotronic effect enhanced Schottky-contact ZnO micro/nanowire humidity sensors. *Nano Res.* **2014**, *7* (7), 1083−1091.
(32) Liu, J.; Zhang, Z.; Qiao, S.; Fu, G.; Wang, S.; Pan, C. Lateral bipolar photoresistance effect in the CIGS heterojunction and its application in position sensitive detector and memory device. *Sci. Bull.* **2020**, *65* (6), 477−485.
(33) Pan, C.; Luo, Z.; Xu, C.; Luo, J.; Liang, R.; Zhu, G.; Wu, W.; Guo, W.; Yan, X.; Xu, J.; Wang, Z. L.; Zhu, J. Wafer-scale high-throughput ordered arrays of Si and coaxial Si/Si(1-x)Ge(x) wires: fabrication, characterization, and photovoltaic application. *ACS Nano* **2011**, *5* (8), 6629−6636.
(34) Sun, J.; Hua, Q.; Zhou, R.; Li, D.; Guo, W.; Li, X.; Hu, G.; Shan, C.; Meng, Q.; Dong, L.; Pan, C.; Wang, Z. L. Piezo-phototronic Effect Enhanced Efficient Flexible Perovskite Solar Cells. *ACS Nano* **2019**, *13* (4), 4507−4513.
(35) Zhang, H.; Peng, D.; Wang, W.; Dong, L.; Pan, C. Mechanically Induced Light Emission and Infrared-Laser-Induced Upconversion in the Er-Doped CaZnOS Multifunctional Piezoelectric Semiconductor for Optical Pressure and Temperature Sensing. *J. Phys. Chem. C* **2015**, *119* (50), 28136−28142.
(36) Zhao, Y.; Gao, W.; Dai, K.; Wang, S.; Yuan, Z.; Li, J.; Zhai, W.; Zheng, G.; Pan, C.; Liu, C.; Shen, C. Bioinspired Multifunctional Photonic-Electronic Smart Skin for Ultrasensitive Health Monitoring, for Visual and Self-Powered Sensing. *Adv. Mater.* **2021**, *33* (45), No. e2102332.
(37) Zhou, R.; Hu, G.; Yu, R.; Pan, C.; Wang, Z. L. Piezotronic effect enhanced detection of flammable/toxic gases by ZnO micro/nanowire sensors. *Nano Energy* **2015**, *12*, 588−596.
(38) Kim, T.-H.; Kim, S.-Y.; Jeon, J.-H.; Choe, H.-H.; Lee, K.-W.; Seo, J.-H.; Shin, J.-H.; Park, S.-H. K.; Hwang, C.-S. P-22: Electrical Stability of ZnO TFT during Gate-Bias Stress. *SID Symp. Dig. Tech. Pap.* **2008**, *39* (1), 1250−1253.
(39) Johansson, R. S.; Vallbo, A. B. Tactile sensibility in the human hand: relative and absolute densities of four types of mechanoreceptive units in glabrous skin. *J. Physiol.* **1979**, *286*, 283−300.
(40) Mantini, G.; Gao, Y. F.; D'Amico, A.; Falconi, C.; Wang, Z. L. Equilibrium Piezoelectric Potential Distribution in a Deformed ZnO Nanowire. *Nano Res.* **2009**, *2* (8), 624−629.
(41) Wang, Z. L. Piezopotential gated nanowire devices: Piezotronics and piezo-phototronics. *Nano Today* **2010**, *5* (6), 540−552.

https://doi.org/10.1021/acsaelm.3c00683
ACS Appl. Electron. Mater. XXXX, XXX, XXX−XXX